Modeling Image Motion in Airborne Three-Line-Array (TLA) Push-broom Cameras

Guimin Jia, Xiangjun Wang, Hong Wei, and Zhaocai Zhang

Abstract

This paper presents an image motion model for airborne three-line-array (TLA) push-broom cameras. Both aircraft velocity and attitude instability are taken into account in modeling image motion. Effects of aircraft pitch, roll, and yaw on image motion are analyzed based on geometric relations in designated coordinate systems. The image motion is mathematically modeled by image motion velocity multiplied by exposure time. Quantitative analysis to image motion velocity is then conducted in simulation experiments. The results have shown that image motion caused by aircraft velocity is space invariant while image motion caused by aircraft attitude instability is more complicated. Pitch, roll, and yaw all contribute to image motion to different extents. Pitch dominates the along-track image motion and both roll and yaw greatly contribute to the cross-track image motion. These results provide a valuable base for image motion compensation to ensure high accuracy imagery in aerial photogrammetry.

Introduction

Aerial photogrammetry is a geomatic method of collecting ground information by using photographic images captured by airborne devices, such as airplanes, helicopters, unmanned airborne vehicles (UAV) or other airborne vehicles (Baltsavias, 1999; Paine and Kiser, 2003; Petrie and Walker, 2007). A line scan camera is one of two principal digital cameras used in aerial photogrammetry, and the other is a frame camera. Generic frame cameras capture an object as a 2D image by using 2D array sensors; while a line scan camera captures an object as a line by using 1D sensors. To create a 2D image with a line scan camera, an object is captured line-by-line by either moving the camera over the object or moving the object under the camera. Compared to a frame camera, a line scan camera usually has higher resolution but low cost, its optics is also simple and compact, and image size is flexible in the along-track direction. A three-line-array (TLA) push-broom camera, which has three linear CCDs being placed in the optical focal plane, can provide 3D information of an object through its stereoscopic views. The TLA push-broom camera is capable of recovering exterior orientation parameters directly from images acquired by itself. It constructs along-track stereoscopy from the same platform with short time intervals so that the failure in image registration caused by changes of lighting condition is avoided to a great extent (Hofmann *et al.*, 1982; Hofmann, 1988; Petrie, 2005; Toutin, 2006; Chen *et al.*, 2007; Petrie and Walker, 2007; Wang *et al.*, 2009).

A Brief History of TLA Cameras

The TLA principle was introduced and patented in the 1980s by the pioneer, Dr. Otto Hofmann (Hofmann *et al.*, 1982; Hofmann, 1985; Hofmann, 1987; Hofmann, 1988). The German Modular Optoelectronic Multispectral Stereo Scanner (MOMS-02) was the first sensor system which used the TLA principle, and in 1993 it was flown on the Space Shuttle Mission STS55 and in 1996 it was installed in the PRIRODA-Module of the MIR Space Station (Fraser and Shao, 1996; Sandau, 2010). Both the High Resolution Stereoscopic (HRS) camera which was equipped on SPOT5 in 2002 and the stereo camera which was installed on Chang'E-1 in 2007 exploited the TLA principle (Toutin, 2006; Sun *et al.*, 2008). With the development of spaceborne TLA cameras, the design of airborne TLA cameras was initiated. The first operational TLA airborne camera system was the Digital Photogrammetry Assembly (DPA). Comprehensive tests were performed by the Institute for Photogrammetry, University of Stuttgart, Germany since 1995. These tests delivered basic experience and knowledge to improve pilot systems to offer operational systems (Fritsch, 1997). The first commercially available digital airborne TLA camera system, ADS40 from Leica Geosystems, was introduced in the year 2000 at the ISPRS Congress in Amsterdam. Through the Position and Orientation System which was designed by Applanix Corporation of Canada, the position information from GPS and the attitude information from the inertial measurement unit (IMU) are combined to provide estimates of the aircraft's trajectory (Sandau, 2010). Indeed, a line scan camera needs to be operated on a very stable imaging platform that does not change its attitude and altitude during flight (Petrie, 2005). Otherwise gaps and double imaging will occur in consecutive strip images. When an airborne platform is subject to atmospheric turbulence, it may cause random and unpredictable changes in attitude and altitude with consequent effects on the imaging system (Sun, 2006). GPS/IMU systems can be used with airborne digital cameras to provide direct georeferencing or to assist in the triangulation process. As a result the accuracy of airborne surveying and mapping is improving.

Guimin Jia, Xiangjun Wang, and Zhaocai Zhang are with the State Key Laboratory of Precision Measuring Technology and Instruments, Tianjin University, No.92 Weijin Road, Nankai District, Tianjin, China, and MOEMS Education Ministry Key Laboratory, Tianjin University, Tianjin, China (gm_j1982@yahoo.com.cn).

Hong Wei is with the School of Systems Engineering, University of Reading, Whiteknights, Reading, RG6 6AY, United Kingdom.

Photogrammetric Engineering & Remote Sensing
Vol. 79, No. 1, January 2013, pp. 000–000.

0099-1112/13/7901–0000/$3.00/0

Research Motivation

There are two conventional lens organizations in TLA cameras: (a) a single lens covering the three linear sensor arrays in its focal plane, and (b) three lenses, each for one linear sensor array, with converging optical axes. The former has advantage of simple mechanical design, while image distortion may be introduced due to edge effects of the lens in a wide-range projection. The latter may acquire high quality images, but its mechanical and optical systems are complex in order to make the three optical axes converge. In Chang'E-1 spacecraft mission, a new type of TLA camera was introduced, in which the three line arrays are selected from 2D CCD arrays using a single lens (Sun *et al.*, 2008). This organization has advantages of compact structure, light weight, and easy assembly. However, it has a longer exposure time compared with purpose-built TLA CCD cameras. Especially when it is used in an airborne platform flying at a high speed (for example reconnaissance missions) with frequent attitude changes, image motion will be significant. This paper analyzes these scenarios with the focus on image motion modeling and simulation.

Image motion is defined as displacement of image points on CCDs caused by relative movement between a camera platform and objects to be captured during image exposure. Two error sources are identified: (a) aircraft velocity, and (b) aircraft attitude instability. This paper first explores the image motion caused by aircraft velocity. Due to angular motion during image exposure, the image motion caused by aircraft velocity is no longer along the flight direction. Second, the image motion caused by attitude instability is modeled by image motion velocity multiplied by exposure time. The image motion velocity is derived from aircraft's pitch, roll, and yaw separately. Finally, simulation experiments are conducted using the established image motion model with detailed analysis with respect to aircraft velocity and attitude instability. The paper ends with conclusions and future research.

Three-line-array Push-broom Camera

As shown in Figure 1, photoelectric imaging elements of a TLA push-broom camera consist of three linear CCD arrays, which are placed in the optical focal plane; *l*, *n*, and *r* stand for forward-looking, nadir-looking, and backward-looking, respectively. The three linear CCD arrays are parallel to each other, and perpendicular to the flight direction. During flight, *l*, *n*, and *r* scan the terrain simultaneously in the same scanning period from different perspectives, thereby produce three overlapping strip images (L_s, N_s, and R_s) (Hofmann, 1988; Hofmann *et al.*, 1982).

It has been proven scientifically that the forward-looking, nadir-looking, and backward-looking views provide sufficient information for photogrammetric reconstruction and stereoscopy is formed by using any pair from the three views (Gruen and Zhang, 2001 and 2002).

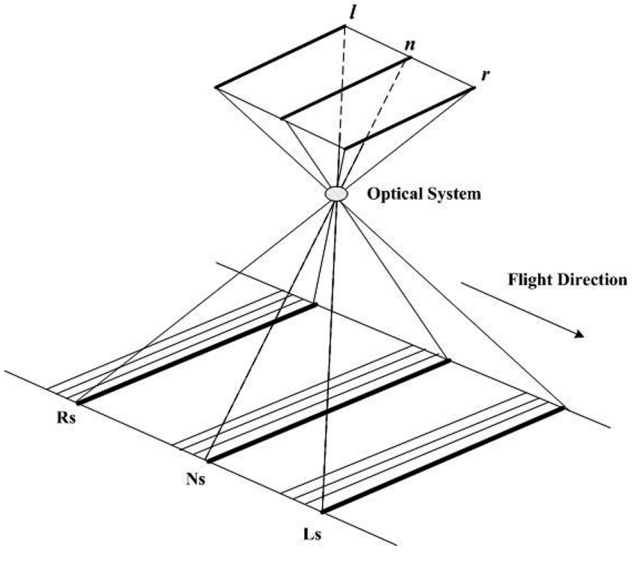

Figure 1. Schematic diagram of three-line-array CCD camera.

Modeling Image Motion in Airborne TLA Push-broom Camera

Establishment of Coordinate Systems

In this paper, four coordinate systems are defined for establishing the computational model of image motion (Refer to Figures 2, 3, 4, and 5 for symbols used in the coordinate systems.):

1. Local geographic coordinate system $F_g(O_g X_g Y_g Z_g)$
   At a point on the Earth's surface, its local geography is treated as flat ground. O_g is a random point on the Earth's surface, axis $O_g X_g$ is parallel to the horizontal, and axis $O_g Z_g$ vertically points to the center of the Earth.
2. Aircraft platform coordinate system $F_b(O_b X_b Y_b Z_b)$
   The aircraft platform coordinate system is fixed to the aircraft, and has its origin at the aircraft's center of gravity. Assuming that the camera is fixed on to the aircraft and the optical center of the lens is also at the center of the aircraft gravity. The camera coordinate system is the same as the aircraft platform coordinate system.

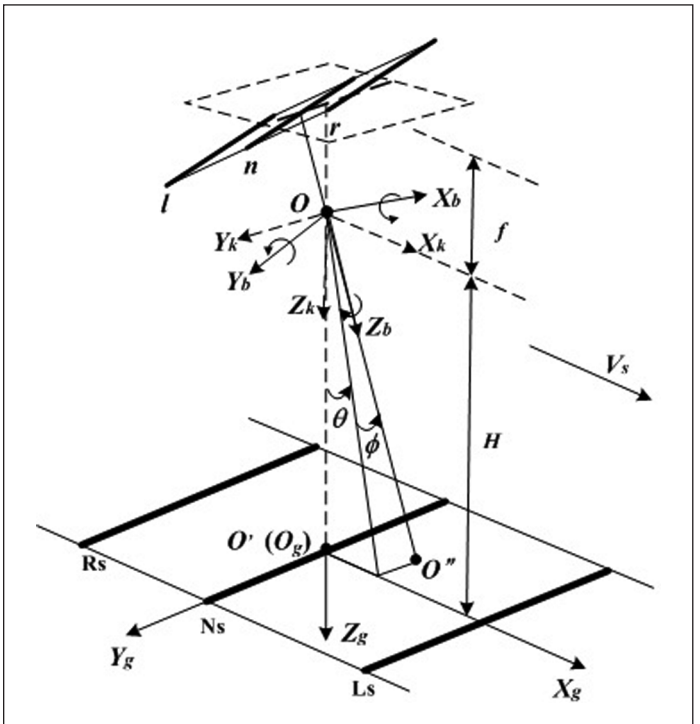

Figure 2. Schematic diagram of image motion caused by aircraft velocity.

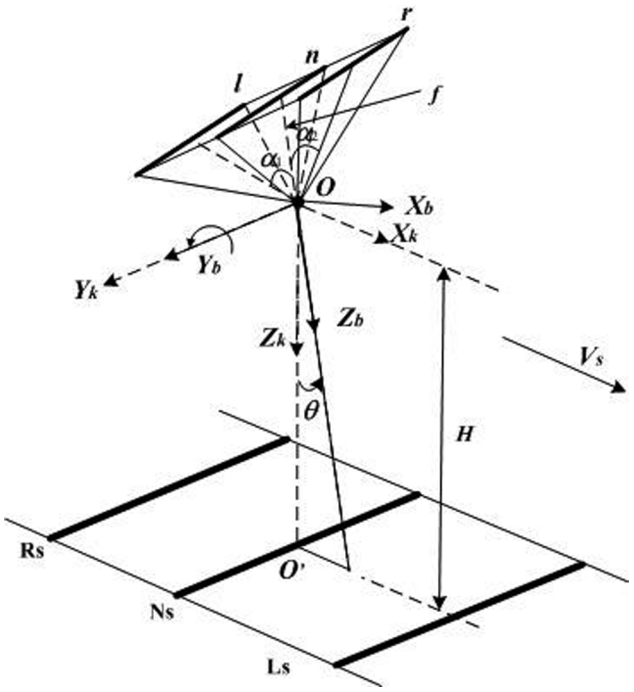

Figure 3. Schematic diagram of image motion caused by pitch.

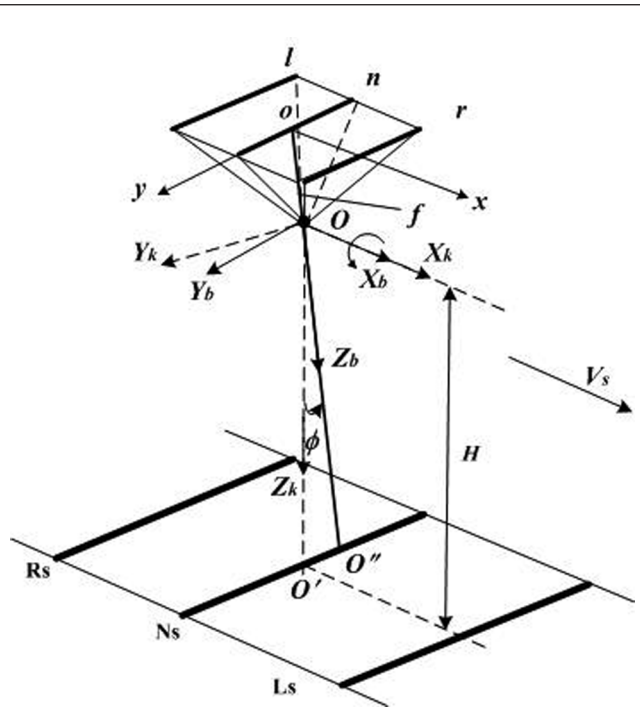

Figure 4. Schematic diagram of image motion caused by roll.

The orientation of the three axes is defined as follows:

1. If the aircraft has a plane of symmetry, then X_b and Z_b lie in that plane. X_b is chosen to point forward stretching from the tail to the nose of the aircraft;

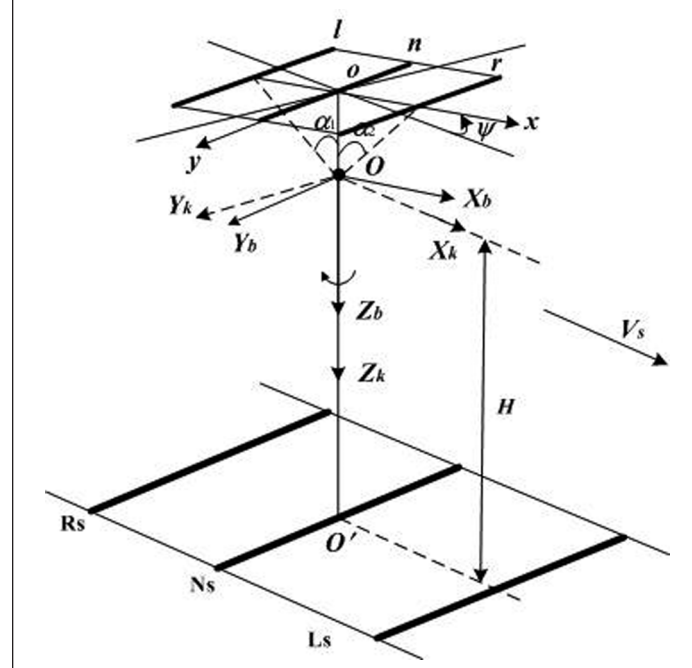

Figure 5. Schematic diagram of image motion caused by yaw.

2. Y_b is a horizontal axis stretching from one wing tip to the other; and
3. Z_b is chosen to point downward and always perpendicular to plane $O_b X_b Y_b$.

The Euler angles, known as yaw, pitch, and roll, describe the attitude and orientation of the aircraft. In this paper, roll is the rotation about $O_b X_b$, pitch refers to the rotation around $O_b Y_b$, and yaw refers to the rotation about $O_b Z_b$. ψ, θ, and ϕ stand for yaw, pitch, and roll, respectively. The positive and negative attitude angles are defined as follows:

1. the clockwise refers to a positive angle when observed along the positive direction of a coordinate axis;
2. otherwise the attitude angle is negative.
3. The flight path coordinate system $F_k(O_k X_k Y_k Z_k)$.
4. The flight path coordinate system has its origin at the aircraft's center of gravity. The $O_k X_k$ axis points to the direction of aircraft velocity. The $O_k Z_k$ axis is in the symmetric plane of the aircraft and points to the Earth's surface.
5. Image plane coordinate system $F_i(oxy)$.

   The image plane coordinate system is a 2D coordinate system, a projection of 3D objects. The origin o lies on the intersection point of the camera optical axis and the image plane, axis ox is parallel to axis $O_b X_b$, and axis oy is parallel to axis $O_b Y_b$. The distance between o and O_b is the focal length f.

Finally, it should be noted that all the coordinate systems are right-handed and orthogonal, and $O_g X_g$ is set to be parallel to $O_k X_k$ in order to simplify the computational model.

Image Motion Modeling

For a camera mounted on a flying aircraft, there is always relative movement between the camera and observed objects during image exposure. When the aircraft flies stably, the

attitude angles (ψ, θ, ϕ) are steady and the aircraft velocity is the primary cause of image motion. When the attitude instability caused by air flows is taken into account, the uncertainty of attitude angles is added into image motion. Image motion caused by both aircraft velocity and attitude instability is analyzed in this section.

Image Motion Caused by Aircraft Velocity

Assuming the attitude angles are steady and set to be zero, the aircraft platform coordinate system F_b is the same as the flight path coordinate system F_k, and the aircraft velocity is along the $O_b X_b$ direction. The image motion δ caused by the aircraft velocity can be calculated by Equation 1 (Prinz, 1985):

$$\delta = f\frac{V_s}{H}\tau \tag{1}$$

where f is the focal length of the imaging system, V_s is the speed of flight, H is the distance between the target object and the CCD camera, and τ is exposure time.

In practice, it is hard to keep the aircraft's attitude angles zero, and there always exist non-zero angles (ψ, θ, ϕ) during image exposure. Therefore Equation 1 is modified to meet the requirement. When the attitude angles are not zero, F_b is no longer the same as F_k. As shown in Figure 2, with attitude angles (ψ, θ, ϕ), the nadir point shifts from O' to O''. The angular motion can be illustrated by coordinate transformations so that the aircraft velocity is transformed from F_k to F_b.

The image motion is mathematically modeled by image motion velocity multiplied by exposure time. The exposure time is constant so that image motion velocity $\vec{\delta}_v$ is used to describe the change rate and direction of image motion. When the attitude angles are (ψ, θ, ϕ) during image exposure, $\vec{\delta}_v$ is calculated based on rotating rules in coordinate systems:

$$\vec{\delta}_v = \delta/\tau = f\frac{\vec{V}}{|OO''|} \tag{2}$$

$$\vec{V} = R_{\psi\theta\phi}\,\vec{V}_s \tag{3}$$

$$|OO''| = H\frac{1}{\cos\theta\cos\phi} \tag{4}$$

where $\vec{V}_s = [V_s, 0, 0]^T$, $R_{\psi\theta\phi}$ is a rotation matrix from the flight path coordinate system F_k to the aircraft platform coordinate system F_b. $R_{\psi\theta\phi}$ can be expressed as:

$$R_{\psi\theta\phi} = R_\phi R_\theta R_\psi$$

$$= \begin{bmatrix} 1 & 0 & 0 \\ 0 & \cos\phi & \sin\phi \\ 0 & -\sin\phi & \cos\phi \end{bmatrix}\begin{bmatrix} \cos\theta & 0 & -\sin\phi \\ 0 & 1 & 0 \\ \sin\phi & 0 & \cos\phi \end{bmatrix}\begin{bmatrix} \cos\psi & \sin\psi & 0 \\ -\sin\psi & \cos\psi & 0 \\ 0 & 0 & 1 \end{bmatrix} \tag{5}$$

Substituting Equation 3, Equation 4, and Equation 5 in Equation 2, the image motion velocity caused by aircraft velocity is obtained as shown in Equation 6:

$$\begin{aligned}\vec{\delta}_v &= [\delta_{vx}, \delta_{vy}]^T \\ &= \Big[f\frac{V_s}{H}\cos\phi\, cos^2\theta\cos\psi, f\frac{V_s}{H}\cos\phi\cos\theta \\ &\qquad (\sin\phi\sin\theta\cos\psi - \cos\phi\sin\psi)\Big]^T\end{aligned} \tag{6}$$

Image Motion Caused by Aircraft Attitude Instability

Image Motion Velocity Caused by Pitch

As shown in Figure 3, α_1 is the angle between the forward-looking and the nadir-looking, α_2 is the angle between the backward-looking and the nadir-looking.

Assuming that pitch θ varies during exposure, and the angular drift rate of pitch is, it can be seen from Figure 3 that the image motion velocity in the across-track direction is zero. Image motion velocity on the three line arrays (l, n, and r) caused by pitch can be computed by Equation 7, Equation 8, and Equation 9, respectively.

$$\vec{\delta}_{\theta l} = [\delta_{\theta lx}, 0]^T = [-\frac{f}{\cos\alpha_1}\dot{\theta}, 0]^T \tag{7}$$

$$\vec{\delta}_{\theta n} = [\delta_{\theta nx}, 0]^T = [-f\dot{\theta}, 0]^T \tag{8}$$

$$\vec{\delta}_{\theta r} = [\delta_{\theta rx}, 0]^T = [-\frac{f}{\cos\alpha_2}\dot{\theta}, 0]^T \tag{9}$$

Image Motion Velocity Caused by Roll

Figure 4 illustrates the aircraft roll. It rolls at an angular drift rate of $\dot{\phi}$, so that the direction of image motion velocity is in the across-track direction or along the oy axis. Image motion velocity on the three line arrays (l, n, and r) caused by roll can be computed by Equation 10, Equation 11, and Equation 12, respectively:

$$\vec{\delta}_{\phi l} = [0, \delta_{\phi ly}] = [0, \sqrt{f^2 + y_l^2}\,\dot{\phi}] \tag{10}$$

$$\vec{\delta}_{\phi n} = [0, \delta_{\phi ny}] = [0, \sqrt{f^2 + y_n^2}\,\dot{\phi}] \tag{11}$$

$$\vec{\delta}_{\phi r} = [0, \delta_{\phi ry}] = [0, \sqrt{f^2 + y_r^2}\,\dot{\phi}] \tag{12}$$

where y_l is the coordinate of the image point on the forward-looking CCD sensor, y_n is the coordinate of the image point on the nadir-looking CCD sensor, and y_r is the coordinate of the image point on the backward-looking CCD sensor.

Image Motion Velocity Caused by Yaw

As shown in Figure5, the aircraft yaws at an angular speed of $\dot{\psi}$. For the forward-looking and backward-looking, the yaw causes motion in both the ox and oy directions. However, the image motion velocity on the nadir-looking CCD is only in the along-track direction or the ox direction. It is calculated by Equation 13:

$$\vec{\delta}_{\psi n} = [\delta_{\psi nx}, 0]^T = [-y_n\,\dot{\psi}, 0]^T \tag{13}$$

The magnitude of forward-looking image motion velocity is calculated by Equation 14:

$$|\vec{\delta}_{\psi l}| = \left|\sqrt{(f\tan\alpha_1)^2 + y_l^2}\,\dot{\psi}\right| \tag{14}$$

where α_1 is the angle between forward-looking and nadir-looking CCD sensors.

The magnitude of backward-looking image motion velocity is calculated by Equation 15:

$$|\vec{\delta}_{\psi r}| = \left|\sqrt{(f\tan\alpha_2)^2 + y_r^2}\,\dot{\psi}\right| \tag{15}$$

where α_2 is the angle between backward-looking and nadir-looking CCD sensors.

Based on the analysis and calculation above, the image motion velocity caused by attitude instability in an airborne TLA push-broom camera is modeled as follows:

1. Forward-looking Sensor

$$\vec{\delta}_{for} = \begin{cases} x\ direction & -\dfrac{f}{\cos\alpha_1}\dot{\theta} - \sin\left(\arctan\dfrac{y_l}{f\tan\alpha_1}\right)\sqrt{(f\tan\alpha_1)^2 + y_l^2}\,\dot{\psi} \\ y\ direction & \sqrt{f^2 + y_l^2}\,\dot{\phi} + \cos\left(\arctan\dfrac{|y_l|}{f\tan\alpha_1}\right)\sqrt{(f\tan\alpha_1)^2 + y_l^2}\,\dot{\psi} \end{cases} \tag{16}$$

2. Nadir-looking Sensor

$$\vec{\delta}_{nadir} = \begin{cases} x\ direction & -f\dot{\theta} - y_n\dot{\psi} \\ y\ direction & \sqrt{f^2 + y_n^2}\,\dot{\phi} \end{cases} \tag{17}$$

3. Backward-looking Sensor

$$\vec{\delta}_{back} = \begin{cases} x\ direction & -\dfrac{f}{\cos\alpha_2}\dot{\theta} - \sin\left(\arctan\dfrac{y_r}{f\tan\alpha_2}\right)\sqrt{(f\tan\alpha_2)^2 + y_r^2}\,\dot{\psi} \\ y\ direction & \sqrt{f^2 + y_r^2}\,\dot{\phi} + \cos\left(\arctan\dfrac{|y_r|}{f\tan\alpha_2}\right)\sqrt{(f\tan\alpha_2)^2 + y_r^2}\,\dot{\psi} \end{cases} \tag{18}$$

Results and Discussion

Equations 6 through 18, have shown that the image motion in an airborne TLA push-broom camera is affected by various factors, such as aircraft velocity, attitude angles, focal length of the imaging system, flight altitude, the angle between forward-looking and nadir-looking CCD sensors, the angle between backward-looking and nadir-looking CCD sensors, and the location of image point on CCD arrays.

Results of Image Motion Caused by Aircraft Velocity

According to reported aerial TLA cameras (Neukum, 1999; Neukum and HRSC-Team, 2001; Tsuno *et al.*, 2004; Sun *et al.*, 2008; Green *et al.*, 2011), parameters involved in this simulation are given as follows: f = 80 mm, V_s = 120 m/s, H = 2500 m, $\alpha_1 = \alpha_2 = 23.02°$, $\dot{\phi} = \dot{\theta} = \dot{\psi} = 0.01$ rad/s, τ = 20 ms, the pixel size of CCD is 6.8 μm, and the number of pixels on each line array is 10,000. According to Equation 6, the image motion velocity caused by aircraft velocity is $\vec{\delta}_v = [3.8324\mu\text{m/ms}, -0.1168\mu\text{m/ms}]^T$, and the magnitude of image motion during exposure is 76.648 μm in the along-track direction and 2.336 μm in the across-track direction. The distribution of image motion velocity caused by aircraft velocity on the three CCD arrays is illustrated in Figure 6.

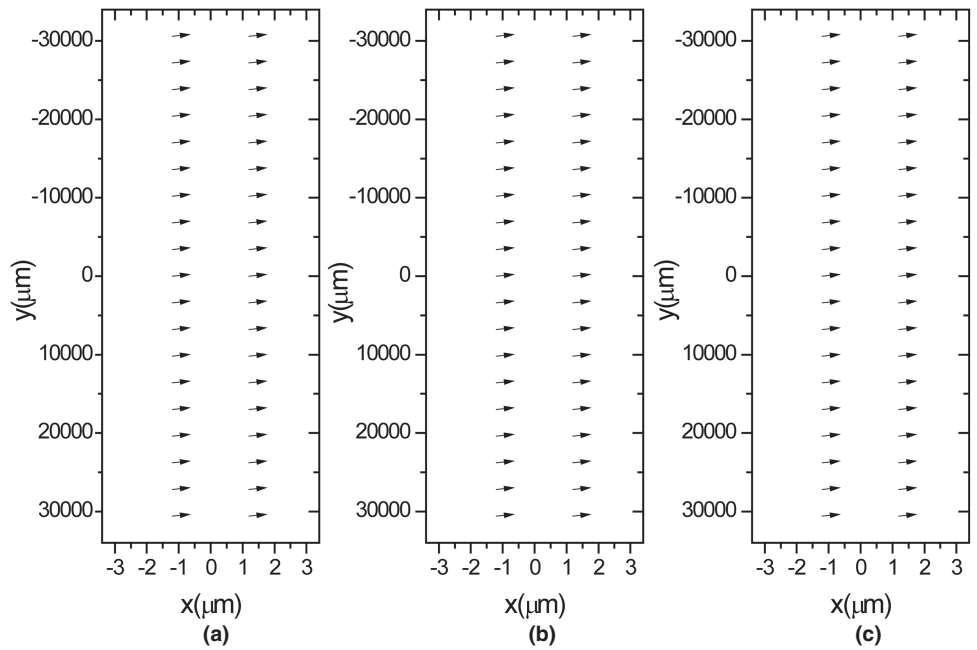

Figure 6. Image motion velocity on (a) forward-looking, (b) nadir-looking, and (c) backward-looking CCD sensors caused by aircraft velocity; the image motion velocity is displayed as arrows. The length of the arrow stands for image motion velocity magnitude, and the direction of the arrow for the motion direction; x and y are the coordinates on the image plane coordinate system.

Figure 6 demonstrates that image motion velocity caused by aircraft velocity is space invariant, and it has the same magnitude and direction on the forward-looking, nadir-looking and backward-looking sensors. With the calculated value from the model, the image motion can be compensated by techniques, such as optical methods, mechanical methods, and TDI (Time Delay and Integrate) method. Furthermore, algorithms used for space invariant image restoration can also be employed as a software method for compensation of this type of image motion.

Results of Image Motion Caused by Attitude Instability

Image motion caused by aircraft attitude instability is more complicated than that caused by aircraft velocity as shown in Equations 16 through 18. In this paper, the analysis is conducted to answer three questions: (a) which CCD array is affected mostly by attitude instability, (b) which attitude angle affects the image motion mostly, and (c) what are features of the image motion when changes of the three attitude angles take place at the same time?

Image Motion Velocity Caused by Pitch, Roll, and Yaw Individually

This simulation intends to discover to what extent the image motion velocity will be introduced by changes of a single attitude angle, hence to indentify which CCD array is affected greatest by attitude instability.

Parameters are given as: $f = 80$ mm, $\dot{\phi} = \dot{\theta} = \dot{\psi} = 0.01$ rad/s, $\alpha_1 = \alpha_2 = 23.02°$. There are 10,000 pixels on a line array sensor. The image motion can be calculated and modeled according to Equations 7 through 15. The distribution of image motion velocity on the forward-looking, nadir-looking, and backward-looking CCDs caused by pitch, roll, and yaw is illustrated in Figures 7, 8, and 9, respectively.

Figure 7 demonstrates that the image motion velocity caused by pitch is space invariant on all the three line array sensors. It points to the along-track direction, and the magnitude is the same for each line array sensor. However the nadir-looking sensor has smaller magnitude than those of the other two line array sensors. In other words, the nadir-looking sensor is less affected by pitch than the forward-looking and backward-looking sensors.

Figure 8 shows that the image motion velocity caused by roll is distributed identically on the three line array sensors. At each point of a line array it is along the across-track direction. Its magnitude is different, and related to image coordinate. The further from the center of the sensor, the greater is the magnitude.

Figure 9 demonstrates the image motion velocity caused by yaw. For the nadir-looking sensor, the image motion velocity is zero at the center of the sensor ($y = 0$). The further from the center, the greater is the magnitude. For the forward-looking and the backward-looking sensors, both magnitude and direction of the image motion velocity vary as a function of image pixel positions at the line array sensor. The further from the center of the sensor, the greater is the magnitude, and the more drifts the image motion velocity direction away from the cross-track direction. Compared to the nadir-looking sensor, the forward-looking and the backward-looking sensors are more seriously affected by aircraft yaw.

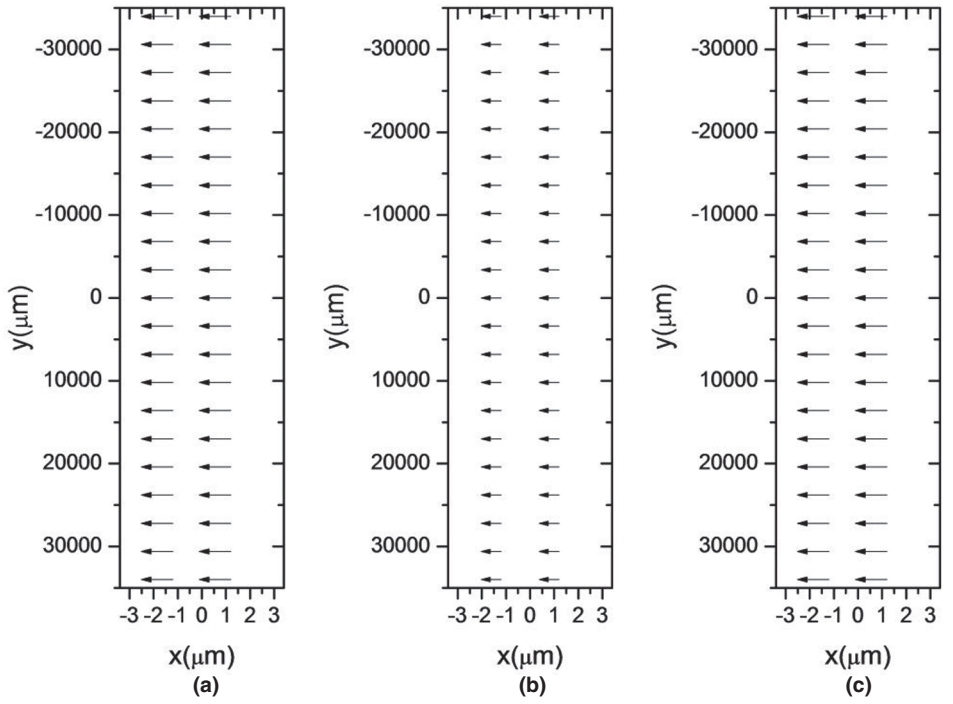

Figure 7. Image motion velocity on (a) forward-looking, (b) nadir-looking, and (c) backward-looking CCD sensors for three line arrays caused by pitch. The image motion velocity is displayed as arrows. The length of the arrow stands for image motion velocity magnitude, and the direction of the arrow stands for the motion direction; x and y are the coordinates in the image plane coordinate system.

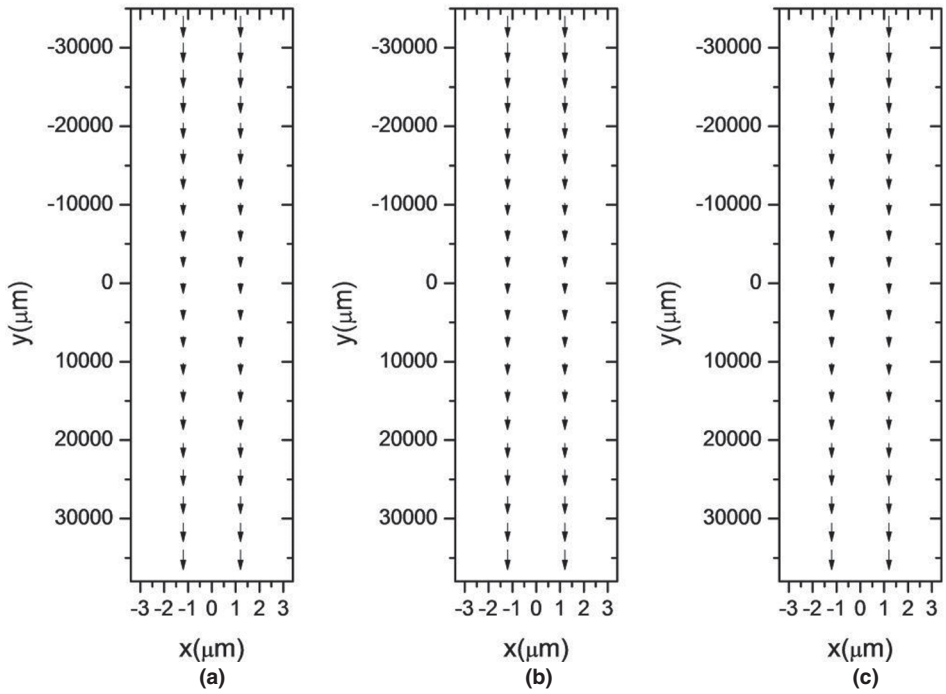

Figure 8. Image motion velocity on (a) forward-looking, (b) nadir-looking, and (c) backward-looking CCD sensors for the three line arrays caused by roll. The image motion velocity is displayed as arrows. The length of the arrow stands for image motion velocity magnitude, and the direction of the arrow stands for the motion direction; *x* and *y* are the coordinates in the image plane coordinate system.

Table 1 shows the simulation results quantitatively. It indicates that the magnitude of image motion velocity caused by attitude instability is smaller for the nadir-looking sensor than for the forward-looking and backward-looking sensors. Among the three attitude angles, yaw has less impact on image motion velocity than pitch and roll.

Image Motion Velocity on One Line Array Caused by Integrated Attitude Changes

This section applies pitch, roll, and yaw simultaneously to one line array sensor. It examines how the uncertainty affects the image motion in individual line array sensors. Assuming that the drifting rate of attitude angles varies from 0.000001 rad/s to 0.05 rad/s, the image motion velocity against it is calculated by Equations 7 through 15 and the results are illustrated in Figure 10.

In the simulation, y_l, y_n, and y_b in Equations 10 through15 are given as 34 mm (0.5 * 6.8 μm * 10,000 pixels, i.e., one-half of the length of pixel array). Figure 10 demonstrates that the image motion velocity magnitude caused by pitch and roll is greater than that caused by yaw. Quantitatively, for the forward-looking sensor, when the angular drifting rate is of 0.01 rad/s, the image motion velocity magnitude caused by yaw is about 0.43 mm/s and that caused by pitch and roll is about 0.85 mm/s. When the angular drifting rate is greater than 0.01 rad/s, the image motion velocity magnitude increases rapidly with increase of the angular drifting rate. For the nadir-looking sensor, at the same angular drifting rate of 0.01 rad/s, the image motion velocity magnitude caused by yaw is about 0.35 mm/s and that caused by pitch and roll is about 0.8 mm/s. Again the image motion magnitude increases rapidly with increase of the angular drifting rate when the angular drifting rate is greater than 0.01 rad/s. For the backward-looking sensor, the trend of image motion velocity magnitude is similar to that of the forward-looking sensor.

TABLE 1. MAGNITUDE OF IMAGE MOTION VELOCITY OF TLA PUSH-BROOM CAMERA CAUSED BY ATTITUDE INSTABILITY

	pitch		roll		yaw	
	Min [μm/ms]	Max [μm/ms]	Min [μm/ms]	Max [μm/ms]	Min [μm/ms]	Max [μm/ms]
Forward-looking	0.869	0.869	0.8	0.869	0.34	0.481
Nadir-looking	0.8	0.8	0.8	0.869	0	0.34
Backward-looking	0.869	0.869	0.8	0.869	0.34	0.481

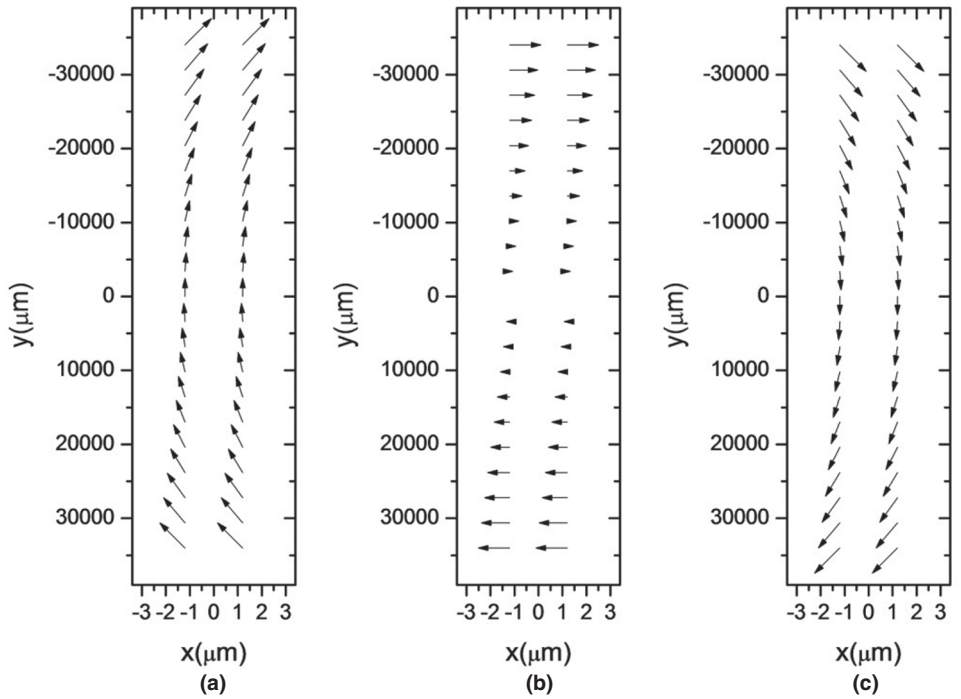

Figure 9. Image motion velocity (a) forward-looking, (b) nadir-looking, and (c) backward-looking CCD sensors for the three line arrays caused by yaw. The image motion velocity is displayed as arrows. The length of the arrow stands for image motion velocity magnitude, and the direction of the arrow stands for the motion direction; x and y are the coordinates in the image plane coordinate system.

From the analysis above, it can be concluded that roll and pitch affect the image motion more than yaw.

Analysis of Image Motion Velocity Caused by Attitude Instability through 3D View

3D views are applied to demonstrate features of the image motion velocity for pitch against yaw, and roll against yaw. This answers the question of which variables (θ, ϕ, ψ, y_l, y_n, y_r) dominate the magnitude and direction of image motion velocity. Taking the forward-looking sensor for example, features of the image motion velocity caused by attitude instability are illustrated in Figures 11 and 12 for motions in the x axis and y axis, respectively. In Figures 11 and 12, the size of symbols represents magnitude. Figure 11 shows that the image motion velocity direction of the forward-looking sensor in the along-track direction is mainly dominated by pitch. The image motion velocity magnitude is affected by y_l, θ, and ψ, among which θ is the major factor. However, the space variance is mainly caused by y_l and ψ. This makes image motion compensation more difficult (Ayasso and Mohammad-Djafari, 2010; Tai *et al.*, 2010).

Figure 12 shows that the image motion velocity direction of the forward-looking sensor in the across-track direction is mainly dominated by roll and yaw. The image motion velocity magnitude is affected by y_l, ϕ, and ψ, among which ϕ and ψ contribute more to the magnitude. The magnitude distribution is also space variant. When roll and yaw change in the same direction (both clockwise or both anticlockwise), the image motion velocity magnitude becomes greater.

Conclusions

In this paper, a computational model is established for airborne TLA push-broom cameras with regard to image motion caused by both aircraft velocity and attitude instability. Aircraft attitude angles (i.e., pitch, roll, and yaw) have been built into the image motion model through four coordinate systems, namely local geographic coordinate system, aircraft platform coordinate system, flight path coordinate system, and image plane coordinate system. The image motion is mathematically modeled in such a way that quantitative analysis can be conducted with given parameters under derived equations. The following conclusions can be made from experimental results based on the computational model of image motion:

- Image motion caused by aircraft velocity is space invariant; both the magnitude and direction of the motion velocity during exposure time are uniform over the image plane regardless image pixel positions.
- Aircraft velocity has the same impact to the forward-looking, nadir looking, and backward-looking sensors with regard to image motion.
- Aircraft pitch (rotation around the y_b axis in the aircraft platform coordinate system) during image exposure introduces greater image motion to the forward-looking and backward-looking sensors than to the nadir-looking sensor. The introduced image motion is also space invariant.
- Aircraft roll (rotation around the x_b axis in the aircraft platform coordinate system) during image exposure has the same impact on the three sensors. However the motion magnitude varies along the y direction.

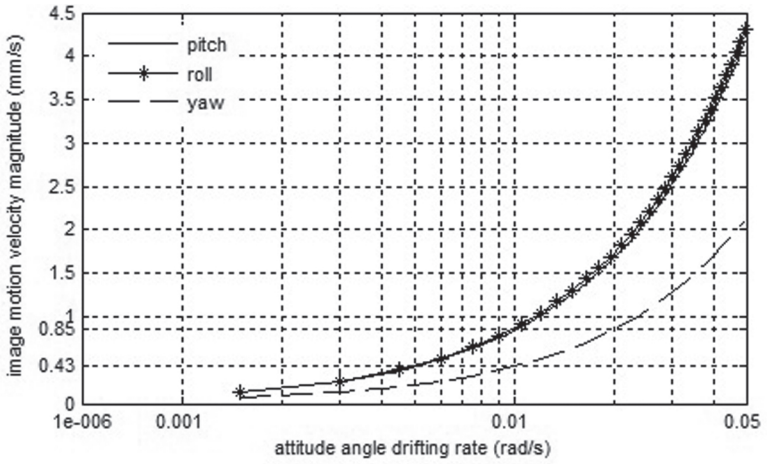

(a)

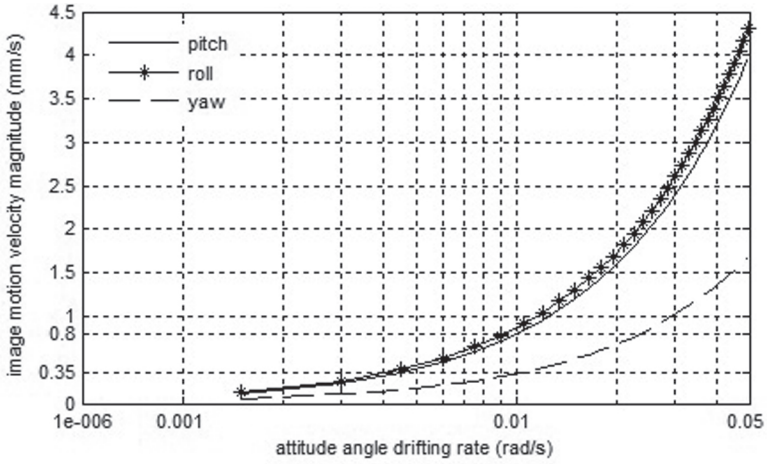

(b)

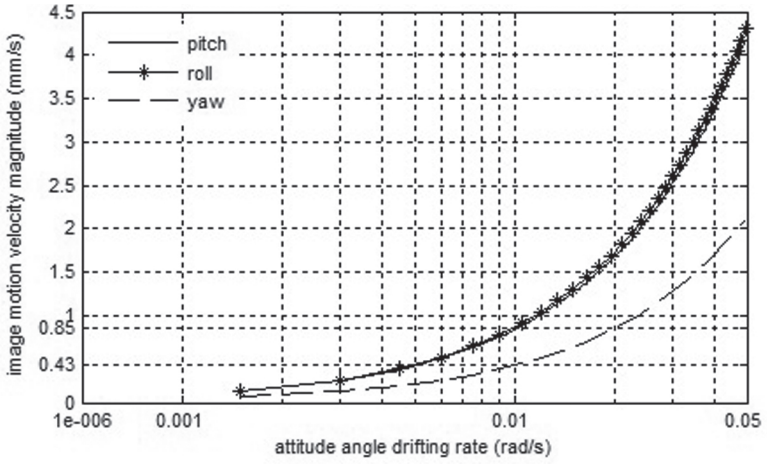

(c)

Figure 10. Comparison of the magnitude of image motion velocity caused by pitch, roll, and yaw: (a) forward-looking, (b) nadir-looking, and (c) backward-looking.

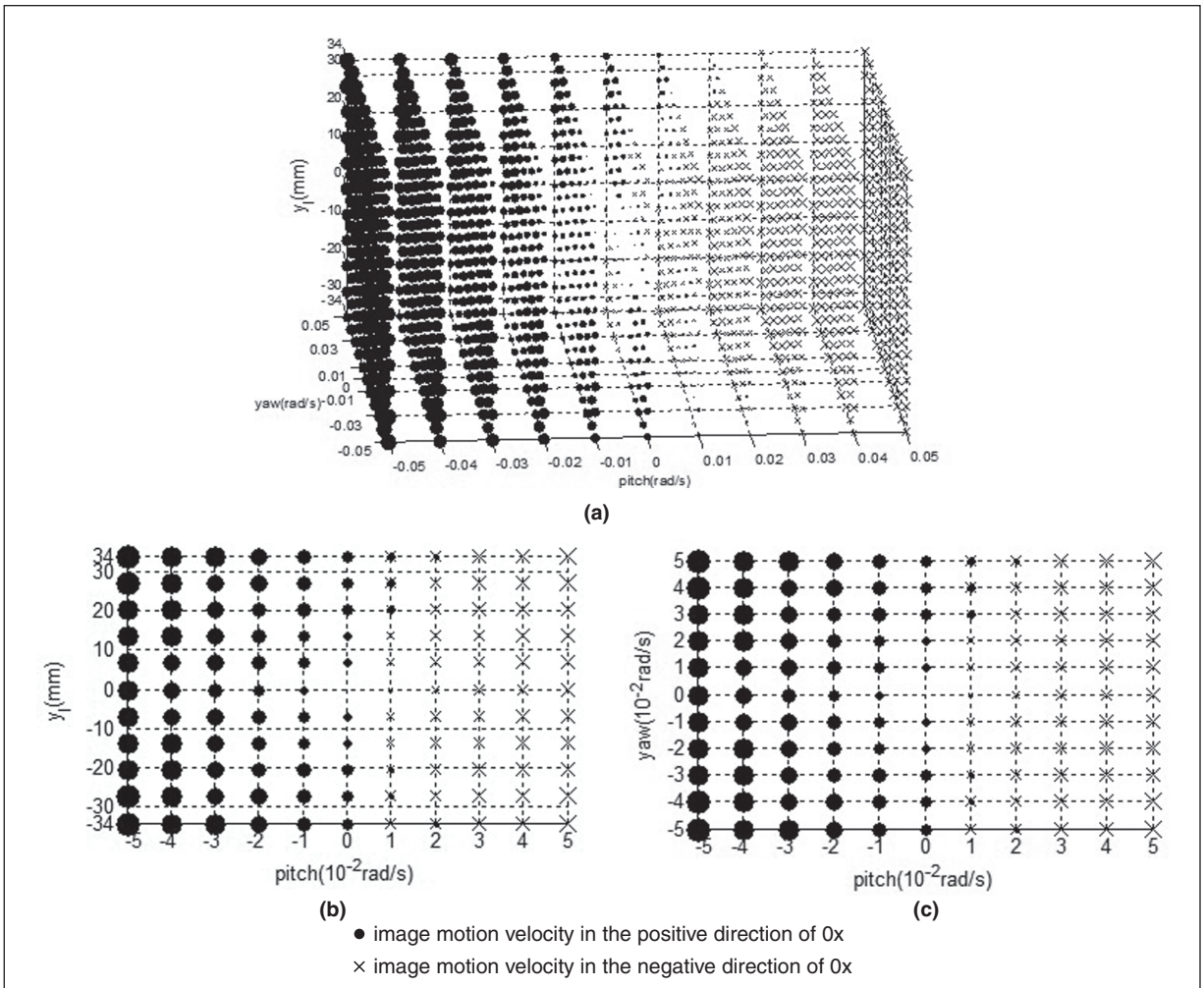

Figure 11. Image motion velocity of the forward-looking sensor in the *ox* direction. (a) 3D view of image motion velocity of the forward-looking sensor in the *ox* direction, (b) front view of (a), and (c) top view of (a).

- Aircraft yaw (rotation around the z_b axis in the aircraft platform coordinate system) during image exposure presents more complicated effects. Both magnitude and direction change with image pixel positions on the image plane. The model provides the detailed equations with which the magnitude and direction of image motion can be calculated at a fixed pixel position. The values can be used for image motion compensation to provide more accurate imagery.
- Among the three variables of pitch, roll, and yaw, yaw has the least effect to image motion. With increase of the attitude angle drifting rate, the image motion velocity is increased, but only after a certain point (0.01 rad/s in the experiment), this trend becomes significant.
- In the *x* direction on the image plane, the aircraft pitch dominates the direction of image motion velocity while both pitch and yaw decide the magnitude.
- In the *y* direction on the image plane, both roll and yaw influence the direction and magnitude of image motion. When roll and yaw change in the same direction (both clockwise or both anticlockwise), the image motion velocity magnitude becomes greater.

The above results can be used in compensation of image motion errors caused by both the aircraft velocity and attitude instability. Quantitative control can be applied to each variable under the image motion model. This is a part of the future work in the project. The work contributes to accurate image registration, stereo matching, and ground point positioning, hence to improve accuracy of aerial photogrammetry by using airborne TLA push-broom cameras.

Acknowledgments

This research was supported by National Natural Science Foundation of China (No. 60872097) and the Key Technologies R&D Program of Tianjin, China (No. 08ZCKFJC27900). The authors are grateful for the anonymous reviewers and the editor's constructive comments to improve the quality of this manuscript.

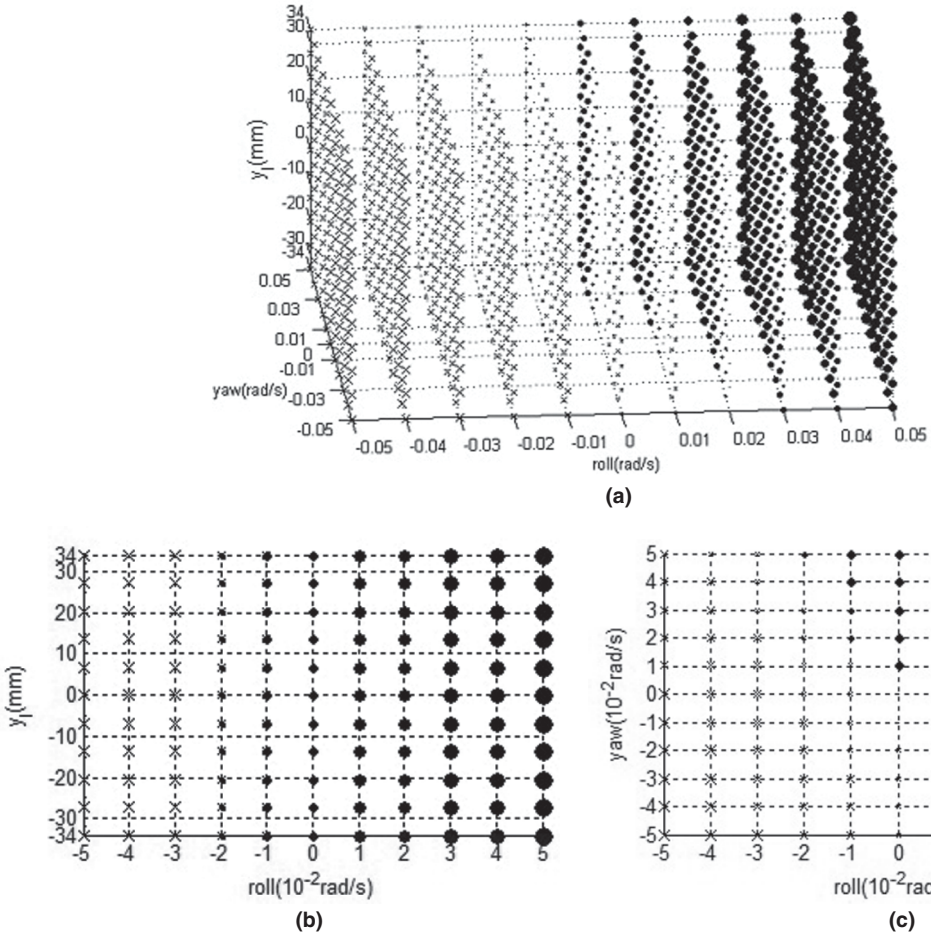

Figure 12. Image motion velocity of forward-looking sensor in the *oy* direction: (a) 3D view of image motion velocity of forward-looking sensor in the *oy* direction, (b) front view of (a), and (c) top view of (a).

References

Ayasso, H., and A. Mohammad-Djafari, 2010. Joint NDT image restoration and segmentation using Gauss-Markov-Potts prior models and variational Bayesian computation, *IEEE Transactions on Image Processing*, 19(9):2265–2277.

Baltsavias, E.P., 1999. A comparison between photogrammetry and laser scanning, *ISPRS Journal of Photogrammetry and Remote Sensing*, 54(2-3):83–94.

Chen, T., R. Shibasaki, and Z. Lin, 2007. A rigorous laboratory calibration method for interior orientation of an airborne linear push-broom camera, *Photogrammetric Engineering & Remote Sensing*, 73(4):369–374.

Fraser, C., and J. Shao, 1996. Exterior orientation determination of MOMS-02 three-line imagery: Experiences with the Australian testfield data, *International Archives of Photogrammetry and Remote Sensing*, 31(B3):207–214.

Fritsch, D., 1997. Experiences with the airborne three-line camera system DPA, *Proceedings of Photogrammetric Week '97* (D. Fritsch and D. Hobbie, editors), Wichmann Verlag, Heidelberg, pp. 63–74.

Green, K., M. Tukman, and M. Finkbeiner, 2011. Comparison of DMC, UltraCam, and ADS40 imagery for benthic habitat and propeller scar mapping, *Photogrammetric Engineering & Remote Sensing*, 77(6):589–599.

Gruen, A., and L. Zhang, 2001. TLS data processing modules, *Proceedings of the 3rd International ImageSensing Seminar on New Developments in Digital Photogrammetry*, 24-27 September, Gifu, Japan, pp. 102–114.

Gruen, A., and L. Zhang, 2002. Automatic DTM generation from three-line-scanner (TLS) images, *International Archives of Photogrammetry and Remote Sensing*, 34(2A):131–137.

Hofmann, O., 1985. Photogrammetric device for aircraft and spacecraft for producing a digital terrain representation, *U.S. Patent 4,504,914*, 12 March 1985.

Hofmann, O., 1987. Device for aircraft and spacecraft for producing a digital terrain representation. *U.S. Patent 4,689,748*, 25 August 1987.

Hofmann, O., 1988. A digital three line stereo scanner system, *International Archives of Photogrammetry and Remote Sensing*, 27(B2):206–213.

Hofmann, O., P. Nave, and H. Ebner, 1982. DPS - A digital photogrammetric system for producing digital elevation models and orthophotos by means of linear array scanner imagery, *International Archives of Photogrammetry and Remote Sensing*, 24(B3):216–227.

Neukum, G., 1999. The airborne HRSC-A: performance results and application potential, *Proceedings of Photogrammetric Week '99* (D. Fritsch and R. Spiller, editors), Wichmann, Heidelberg, pp. 83–88.

Neukum, G., and the HRSC-Team, 2001. The airborne HRSC-AX cameras: evaluation of the technical concept and presentation of application results after one year of operations, *Proceedings of Photogrammetric Week '2001* (D. Fritsch and R. Spiller, editors), Wichmann, Heidelberg, pp. 117–130.

Paine, D.P., and J.D. Kiser, 2003. *Aerial Photography and Image* Interpretation, second edition), John Wiley & Sons, Inc., Hoboken, New Jersey.

Petrie, G., 2005. Airborne pushbroom line scanners: an alternative to digital frame cameras, *GeoInformatics*, 8(1):50–57.

Petrie, G., and A.S. Walker, 2007. Airborne digital imaging technology: a new overview, *The Photogrammetric Record*, 22(119):203–225.

Prinz, R.. Method and means for compensating for image motion in an aerial camera, *U.S. Patent 4,505,559*, 19 March 1985.

Sandau, R., 2010. *Digital Airborne Camera: Introduction and Technology*, Springer Dordrecht Heidelberg, London, pp. 1–29.

Sun, H., 2006. Introduction to GPS/IMU integration, *Photogrammetric Engineering & Remote Sensing*, 72(2):90–92.

Sun, H., J. Wu, S. Dai, B. Zhao, R. Shu, J. Chang, H. Wang, X. Zhang, Q. Ren, X. Chen, Z. Ouyang, and Y. Zou, 2008. Introduction to the payloads and the initial observation results of Chang'E-1, *Chinese Journal of Space Science*, 28(5):374–384.

Tai, Y., H. Du, M.S. Brown, and S. Lin, 2010. Correction of spatially varying image and video motion blur using a hybrid camera, *IEEE Transactions on Pattern Analysis and Machine Intelligence*, 32(6):1012–1028.

Toutin, T., 2006. Generation of DSMs from SPOT-5 in-track HRS and across-track HRG stereo data using spatiotriangulation and autocalibration, *ISPRS Journal of Photogrammetry and Remote Sensing*, 60(3):170–181.

Tsuno, K., A. Gruen, L. Zhang, S. Murai, and R. Shibasaki, 2004. StarImager - A new airborne three-line scanner for large-scale applications, *International Archives of Photogrammetry and Remote Sensing*, 35(B1):226–231.

Wang, M., F. Hu, J. Li, and J. Pan, 2009. A fast approach to best scanline search of airborne linear pushbroom images, *Photogrammetric Engineering & Remote Sensing*, 75(9):1059–1067.

(Received 14 October 2011; accepted 13 september 2012; final version 26 September 2012)